Supplementary data

Targeting Ubiquitin-Like Protein, ISG15, as a Novel Tumor-Associated Antigen in Colorectal Cancer

Hong-My Nguyen, Shreyas Gaikwad, Mariam Oladejo, Wyatt Paulishak, Laurence M Wood

Department of Immunotherapeutics and Biotechnology, Jerry H Hodge School of Pharmacy,
Texas Tech University Health Sciences Center, Abilene, TX 79601, USA
* Correspondence: laurence.wood@ttuhsc.edu; Tel.: +1-(325)-696-0431

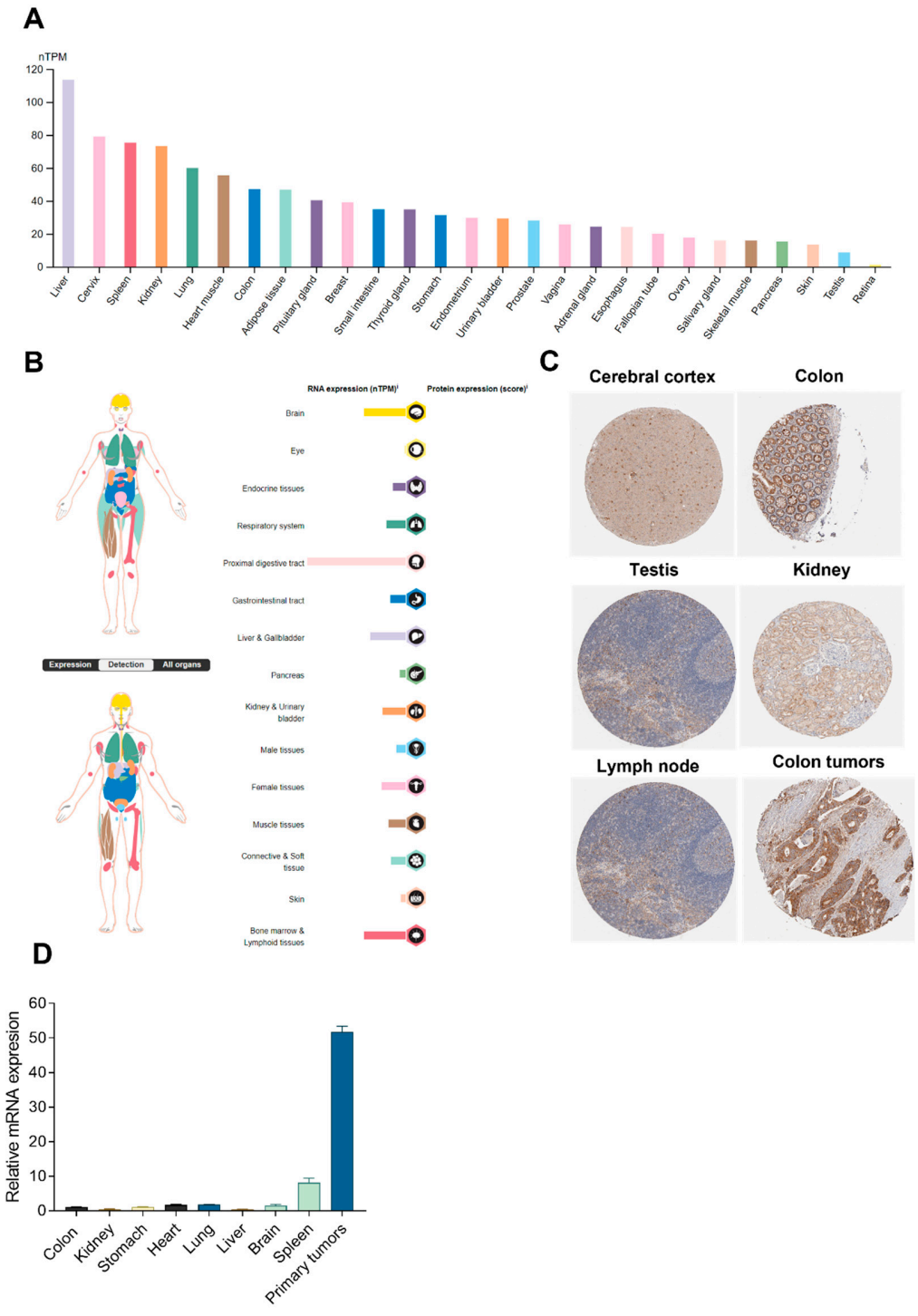

Supplementary Figure S1. ISG15 expression at transcriptional and translational expression. (**A**) Human ISG15 mRNA expression from GTEx dataset, (**B**) mRNA and protein expression of ISG15 in different healthy tissues, (**C**) Immunohistochemistry staining of ISG15 in different healthy organs and CRC tumor. (**D**) mRNA expression of ISG15 in different organs of C57BL/6 female mice.

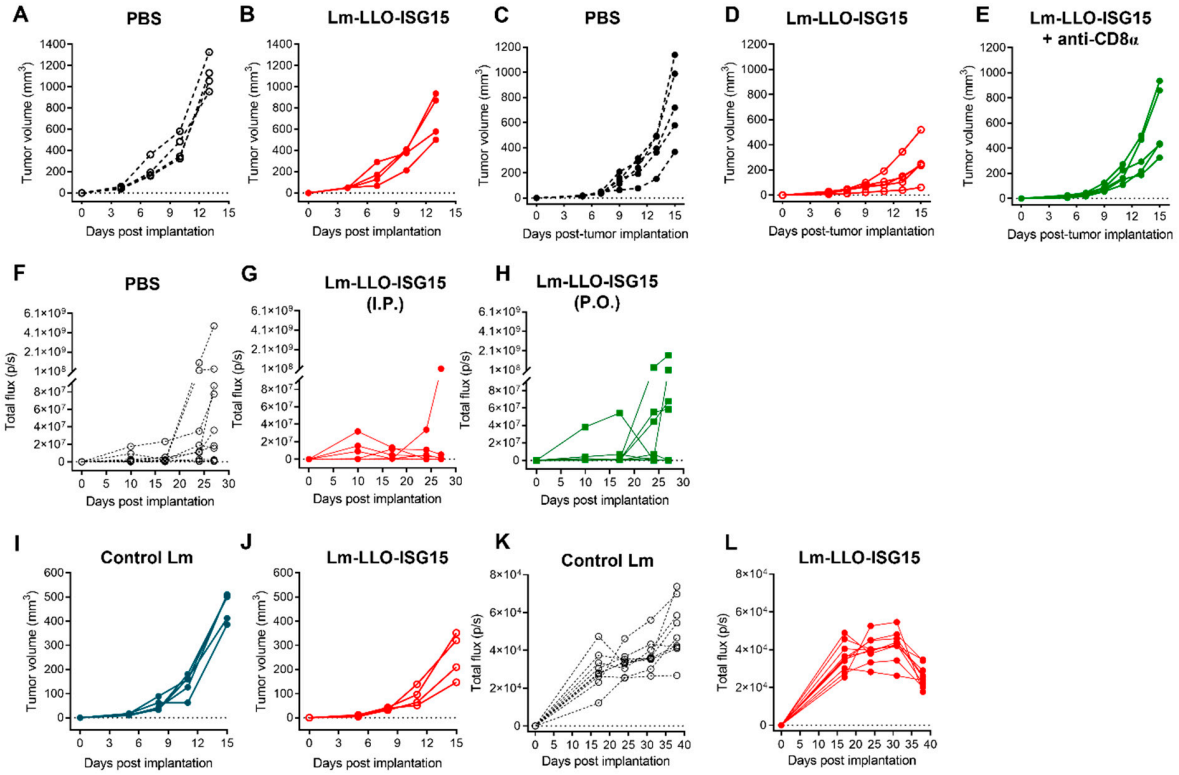

Supplementary Figure S2. Individual tumor growth kinetics of (**A-B**) experiment 3B, (**C-E**) experiment 3M, (**F-H**) experiment 4B, (**I-J**) experiment 5B, and (**K-L**) experiment 5F.

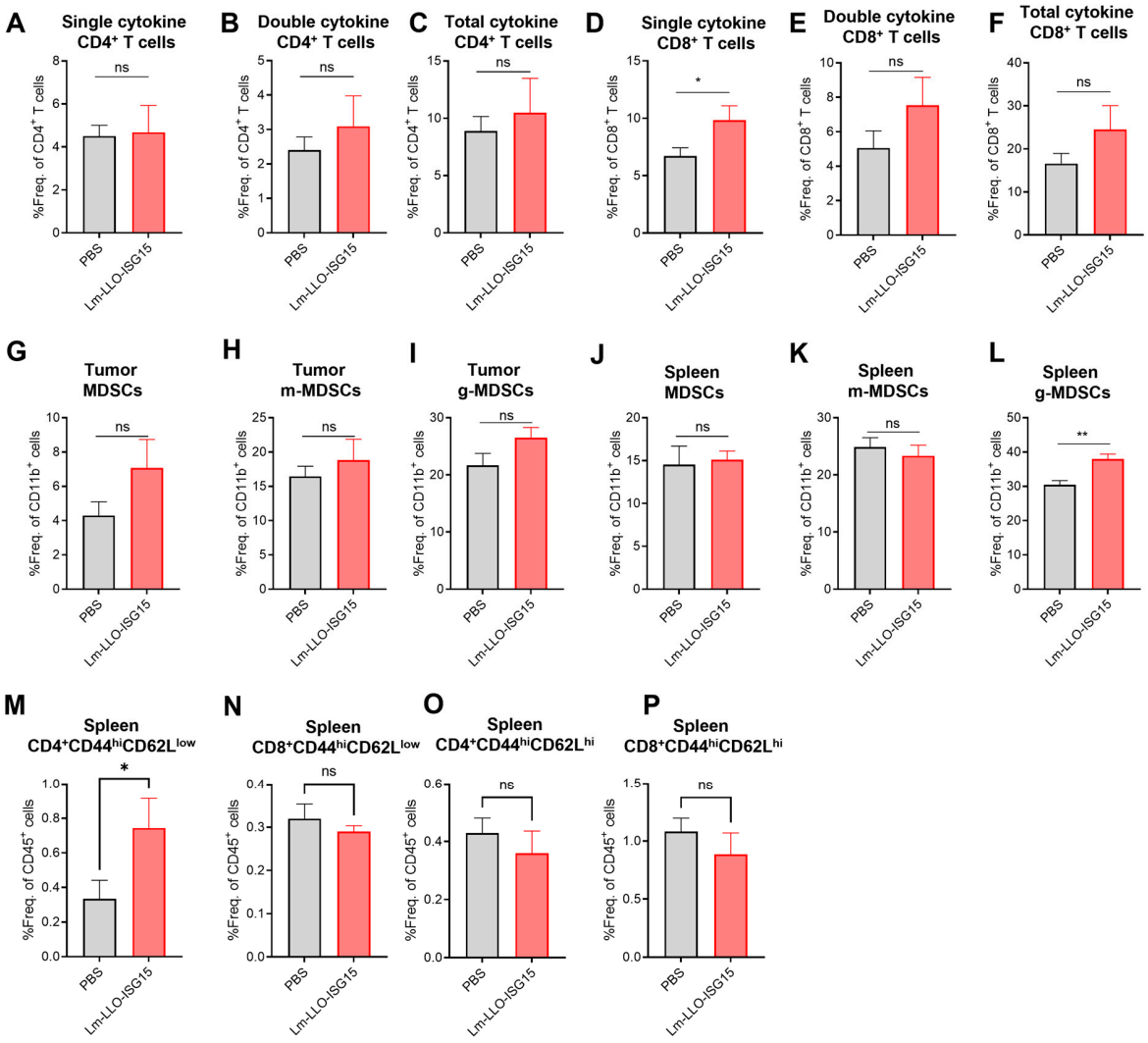

Supplementary Figure S3. Lm-LLO-ISG15 exerts an anti-tumor efficacy in subcutaneous CRC mouse model. Tumors and spleens from experiment **3A** were harvested, dissociated to single cells, and subjected to multicolor flow cytometry as described in section Materials and methods. (**A**) Frequency of live $CD4^+IFN\text{-}\gamma^+$ and $CD4^+IL\text{-}2^+$ and $CD4^+TNF\text{-}\alpha^+$, (**B**) Frequency of live $CD4^+IFN\text{-}\gamma^+IL\text{-}2^+$ and $CD4^+IL\text{-}2^+TNF\text{-}\alpha^+$ and $CD4^+IFN\text{-}\gamma^+TNF\text{-}\alpha^+$, (**C**) Frequency of live $CD4^+$ T cells from S1A and S1B and $CD4^+IFN\text{-}\gamma^+IL\text{-}2^+TNF\text{-}\alpha^+$, (**D**) Frequency of live $CD8^+IFN\text{-}\gamma^+$ and $CD8^+IL\text{-}2^+$ and $CD8^+TNF\text{-}\alpha^+$, (**E**) Frequency of live $CD8^+IFN\text{-}\gamma^+IL\text{-}2^+$ and $CD8^+IL\text{-}2^+TNF\text{-}\alpha^+$ and $CD8^+IFN\text{-}\gamma^+TNF\text{-}\alpha^+$, (**F**) Frequency of live $CD8^+$ T cells from S1D and S1E and $CD8^+IFN\text{-}\gamma^+IL\text{-}2^+TNF\text{-}\alpha^+$, (**G, J**) Frequency of live $CD11b^+Gr1^+$, (**H, K**) Frequency of live $CD11b^+Gr1^{hi}$, (**I,L**) Frequency of live $CD11b^+Gr1^{int}$, (**M**) Frequency of live $CD4^+CD44^{hi}CD62L^{low}$, (**N**) Frequency of live $CD8^+CD44^{hi}CD62L^{low}$, (**O**) Frequency of live $CD4^+CD44^{hi}CD62L^{hi}$, (**P**) Frequency of live $CD8^+CD44^{hi}CD62L^{hi}$.

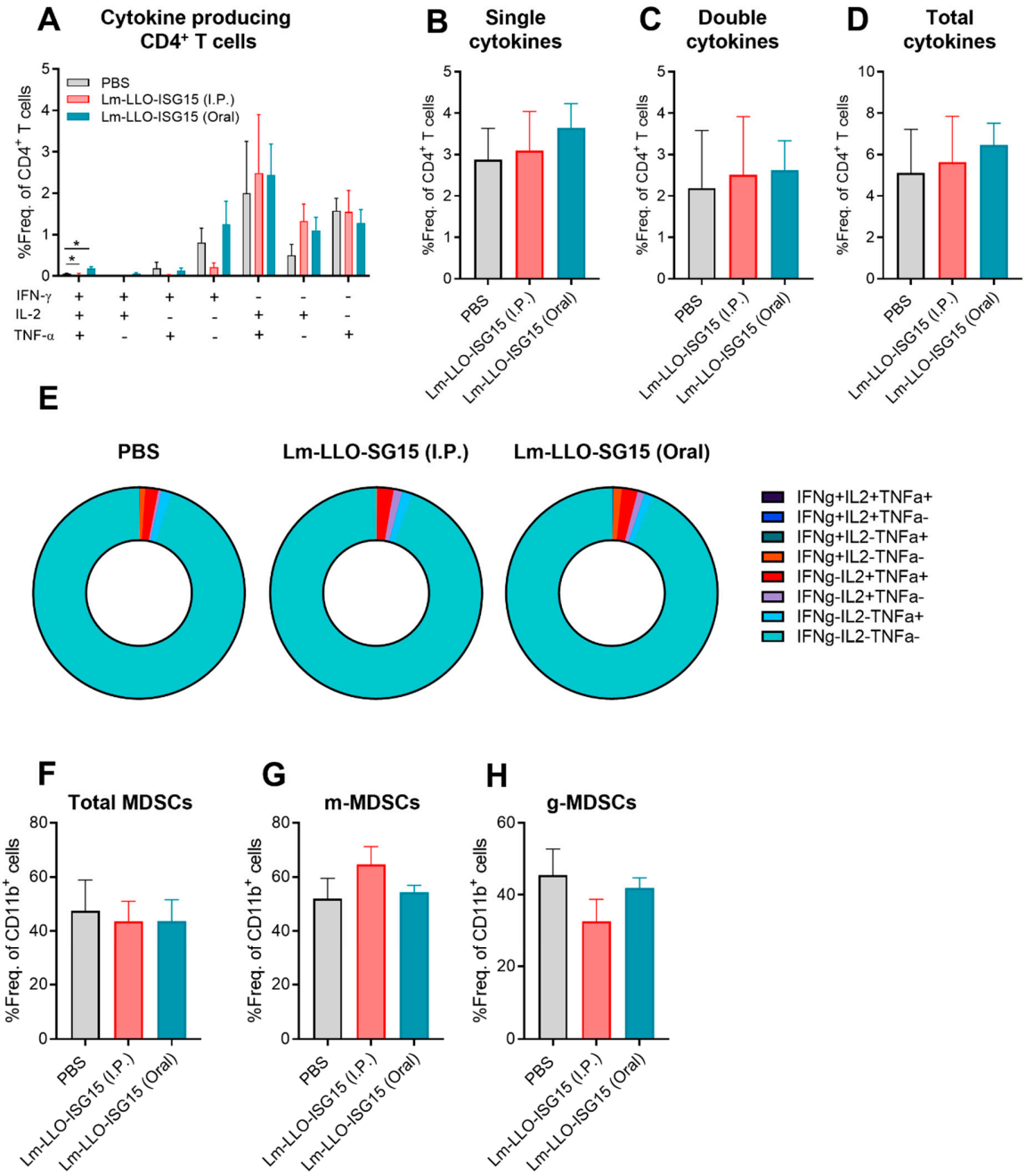

Supplementary Figure S4. Lm-LLO-ISG15 exerts an anti-tumor efficacy in orthotopic CRC mouse model. Tumors from experiment **4A** were harvested, dissociated to single cells, and subjected to multicolor flow cytometry as described in section Materials and methods. (**A, E**) Distribution of multi-cytokine produced by live $CD4^+$ T cells. (**B**) Frequency of live $CD4^+IFN\text{-}\gamma^+$ and $CD4^+IL\text{-}2^+$ and $CD4^+TNF\text{-}\alpha^+$, (**C**) Frequency of live $CD4^+IFN\text{-}\gamma^+IL\text{-}2^+$ and $CD4^+IL\text{-}2^+TNF\text{-}\alpha^+$ and $CD4^+IFN\text{-}\gamma^+TNF\text{-}\alpha^+$, (**D**) Frequency of live $CD4^+$ T cells from S2B and S2C and $CD4^+IFN\text{-}\gamma^+IL\text{-}2^+TNF\text{-}\alpha^+$, (**F**) Frequency of live $CD11b^+Gr1^+$, (**G**) Frequency of live $CD11b^+Gr1^{hi}$, (**H**) Frequency of live $CD11b^+Gr1^{int}$.

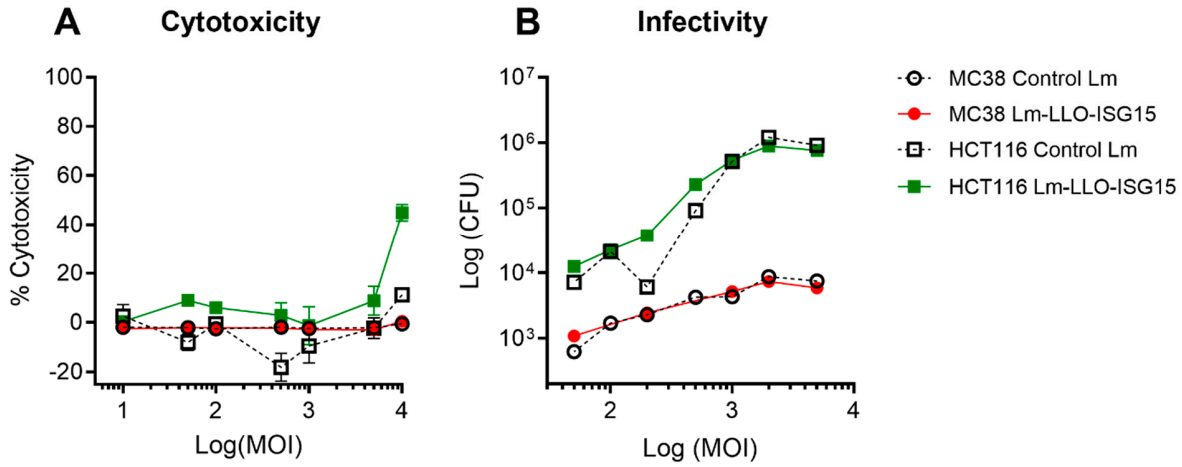

Supplementary Figure S5. Direct killing effect or invasive capacity of *Lm*-based vaccines. MC38 and HCT116 cells were cultured with varying MOIs of Control Lm or Lm-LLO-ISG15, and (**A**) Dose-response curve or (**B**) Infectivity rate, were determined.

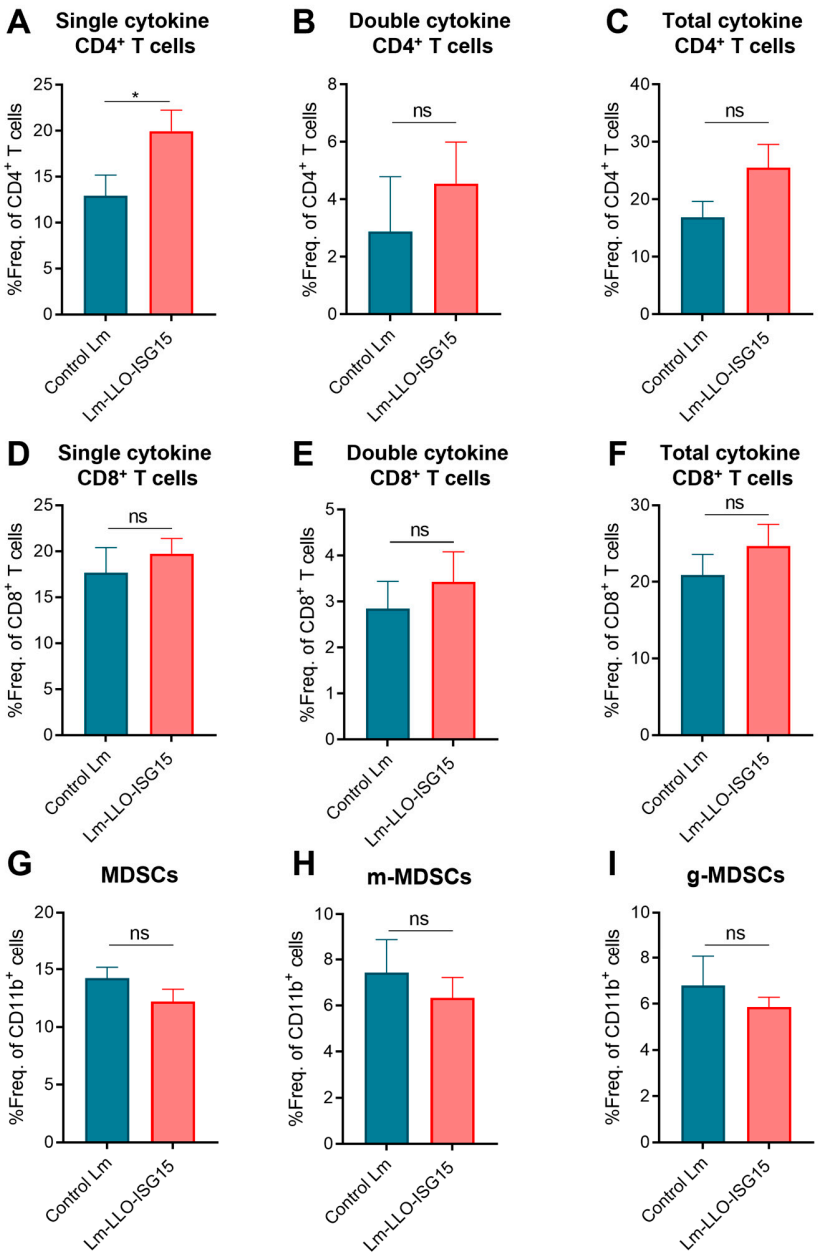

Supplementary Figure S6. Lm-LLO-ISG15 exerts an anti-tumor efficacy in subcutaneous CRC mouse model in comparison to Control Lm. Tumors and spleens from experiment **5A** were harvested, dissociated to single cells, and subjected to multicolor flow cytometry as described in section Materials and methods. (**A**) Frequency of live CD4$^+$IFN-γ^+ and CD4$^+$IL-2$^+$ and CD4$^+$TNF-α^+, (**B**) Frequency of live CD4$^+$IFN-γ^+IL-2$^+$ and CD4$^+$IL-2$^+$TNF-α^+ and CD4$^+$IFN-γ^+TNF-α^+, (**C**) Frequency of live CD4$^+$ T cells from S4A and S4B and CD4$^+$IFN-γ^+IL-2$^+$TNF-α^+, (**D**) Frequency of live CD8$^+$IFN-γ^+ and CD8$^+$IL-2$^+$ and CD8$^+$TNF-α^+, (**E**) Frequency of live CD8$^+$IFN-γ^+IL-2$^+$ and CD8$^+$IL-2$^+$TNF-α^+ and CD8$^+$IFN-γ^+TNF-α^+, (**F**) Frequency of live CD8$^+$ T cells from S4D and S4E and CD8$^+$IFN-γ^+IL-2$^+$TNF-α^+, (**G**) Frequency of live CD11b$^+$Gr1$^+$, (**H**) Frequency of live CD11b$^+$Gr1^{hi}, (**I**) Frequency of live CD11b$^+$Gr1^{int}

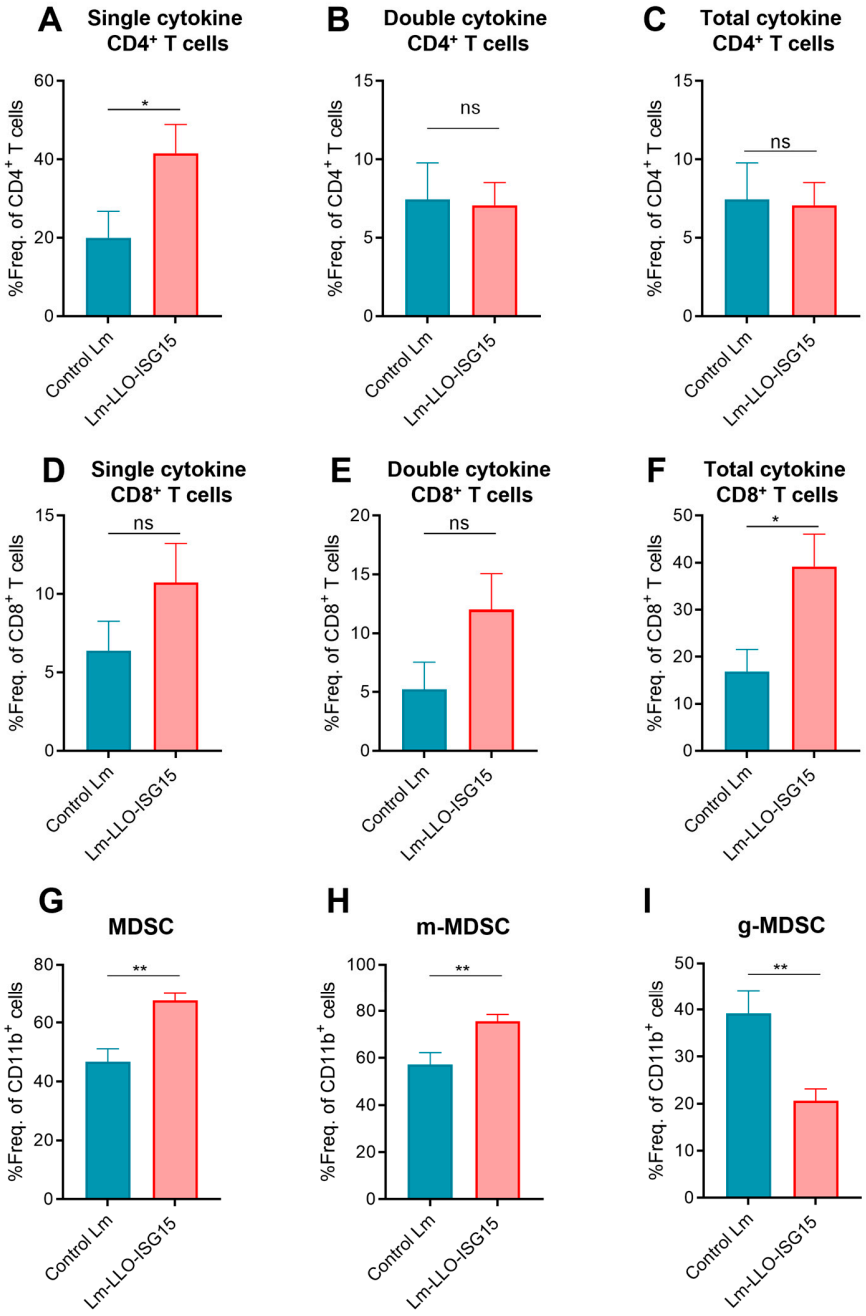

Supplementary Figure S7. Lm-LLO-ISG15 exerts an anti-tumor efficacy in subcutaneous CRC mouse model in comparison to Control Lm. Tumors and spleens from experiment **5E** were harvested, dissociated to single cells, and subjected to multicolor flow cytometry as described in section Materials and methods. (**A**) Frequency of live $CD4^+IFN\text{-}\gamma^+$ and $CD4^+IL\text{-}2^+$ and $CD4^+TNF\text{-}\alpha^+$, (**B**) Frequency of live $CD4^+IFN\text{-}\gamma^+IL\text{-}2^+$ and $CD4^+IL\text{-}2^+TNF\text{-}\alpha^+$ and $CD4^+IFN\text{-}\gamma^+TNF\text{-}\alpha^+$, (**C**) Frequency of live $CD4^+$ T cells from S5A and S5B and $CD4^+IFN\text{-}\gamma^+IL\text{-}2^+TNF\text{-}\alpha^+$, (**D**) Frequency of live $CD8^+IFN\text{-}\gamma^+$ and $CD8^+IL\text{-}2^+$ and $CD8^+TNF\text{-}\alpha^+$, (**E**) Frequency of live $CD8^+IFN\text{-}\gamma^+IL\text{-}2^+$ and $CD8^+IL\text{-}2^+TNF\text{-}\alpha^+$ and $CD8^+IFN\text{-}\gamma^+TNF\text{-}\alpha^+$, (**F**) Frequency of live $CD8^+$ T cells from S5D and S5E and $CD8^+IFN\text{-}\gamma^+IL\text{-}2^+TNF\text{-}\alpha^+$, (**G**) Frequency of live $CD11b^+Gr1^+$, (**H**) Frequency of live $CD11b^+Gr1^{hi}$, (**I**) Frequency of live $CD11b^+Gr1^{int}$

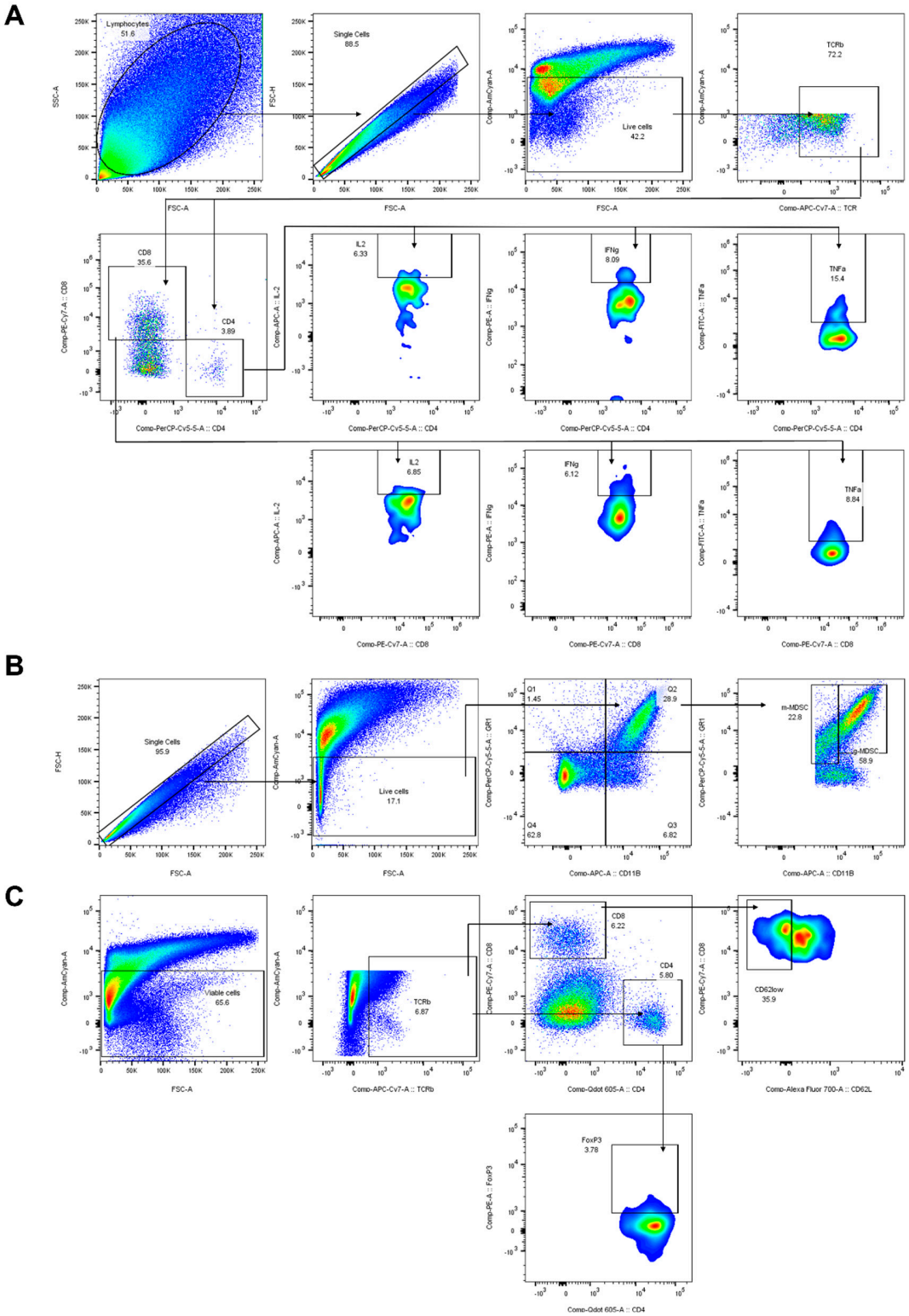

Supplementary Figure S8. Gating strategies for tumor-infiltrating lymphocytes and myeloid cells.